Carbon 179 (2021) 677–682

Contents lists available at ScienceDirect

Carbon

journal homepage: www.elsevier.com/locate/carbon

Research Article

Evidence of flexoelectricity in graphene nanobubbles created by tip induced electric field

Rajarshi Roy [a, *], David Nečas [b], Lenka Zajíčková [b, c]

[a] CEITEC, Masaryk University, Brno, 62500, Czech Republic
[b] CEITEC, Brno University of Technology, Purkyňova 123, 61200, Czech Republic
[c] Department of Condensed Matter Physics, Faculty of Science, Masaryk University, Kotlářská, Brno, 61137, Czech Republic

ARTICLE INFO

Article history:
Received 11 February 2021
Received in revised form
14 April 2021
Accepted 26 April 2021
Available online 29 April 2021

Keywords:
Graphene nanobubbles
Piezoelectric force microscopy
Flexoelectricity

ABSTRACT

Strain engineering in graphene nanobubbles (GNB) has made significant progress in recent years opening new possibilities to observe quantum phenomena such as Newton's ring oscillation and generation of pseudomagnetic field. Here, we demonstrated that controlled formation of graphene nanobubbles is possible on transferred graphene on standard SiO_2/Si substrate by the application of external electric field through the tip of piezoelectric force microscope (PFM). We manipulated their dimensional attributes (height, area and volume) by varying tip ramp voltage and tip distance. Prominent out-of-plane piezo-response (flexoelectricity) was observed using PFM in the newly created nanobubbles due to the presence of non-uniform strain gradients in the nanobubbles. Moreover, we found quadratic dependence of the effective piezoelectric coefficient proportional to the increasing bubble creation ramp voltage. Our work motivates the exploration of flexoelectric properties and related applications with 2D nanobubbles on different substrates.

1. Introduction

The transfer of single layer graphene [1,2] on different substrates (e.g. 285 nm SiO_2/Si) often causes the formation of minute bulges (a few hundred nanometers up to several microns) on the SLG surface, reminiscent of the so-called graphene bubbles or blisters [3,4]. These structures originate from the entrapment of air molecules between the SLG sheet and the underneath substrate and have shown fascinating optical properties in the recent years [3,5]. For example, optical standing waves formed in the vicinity of the graphene surface are reported in large graphene bubbles with spectral signature of size dependent oscillations in intensity and frequency in the Raman spectra [5]. The curvature of the graphene bubbles is known to vary with applied external electric field. This effect can be used for adaptive lensing applications [3]. Moreover, under the influence of anisotropic strain gradient the bubbles can generate quasi-constant pseudomagnetic field and manifest further opening of band gap [6,7]. In fact, strain engineering in graphene have been shown to influence the electronic properties significantly, paving the way to the investigation of piezoelectricity in graphene. The centrosymmetric crystal structure of graphene prohibits the exhibition of any piezo property in its pristine state. However, it can be induced by breaking the inversion symmetry by doping, in-line defects or deformations which lead to specific strain gradients and internal polarization within the material [8–13]. It was observed that vertical piezoresponse in suspended graphene sheets were able to yield a high piezoelectric coefficient that is comparable to traditional well-known piezo materials such as lead zirconium titanate (PZT) [8]. Since then many 2D materials were predicted to exhibit large piezoelectric effects [14–16]. Recent reports regarding the out-of-plane piezoresponse in MoS_2 and other transition metal dichalcogenides [17–20] also provide further such evidence. Moreover, piezoelectricity in monolayer hexagonal boron nitride bubbles was reported where non-uniform strain induced charge density ρ is expected to appear due to the variation in the local polarization P, since $\rho(r) = -\nabla.P(r)$. [21,22] Furthermore, theoretical investigation of flexoelectricity in crumpled thin sheets by Wang et al. [23] established scaling laws for their electromechanical behavior to prove that an extremely strong flexoelectric response is achieved at submicron length scales. Zhuang et al. [24] proposed a theoretical mechanical bending scheme that eliminates the piezoelectric contribution to the total polarization, which facilitated the direct measurements of the flexoelectric constants.

* Corresponding author.
E-mail address: rajarshiroy84@gmail.com (R. Roy).

https://doi.org/10.1016/j.carbon.2021.04.086
0008-6223/

Moreover, while flat 2D materials like graphene have low flexoelectric constants due to weak π-σ interactions, buckling is found to increase the flexoelectric constants in monolayer group-IV elements. Low-dimensional biological membranes and 2D hollow spheres have emerged with excellent flexoelectric response from a wide range of applications such as nano-generators, artificial muscles, micro-robots and MEMS [25,26]. In recent years, aligned GaN nanorod on graphene sheets have been demonstrated as a potential candidate for transparent piezoelectric flexoelectric material with a wide range of applicability as self-powered nano/biosensors, and piezo-phototronic effect enhanced solar cells and light-emitting diodes [27].

It is well-known that applying a voltage from an atomic force microscopy (AFM) tip can modify the surface of SLG by deformation and/or electrochemical processes [28]. However, the bigger question is whether it can also create a bubble with possibility of piezoelectricity? Recently Jia et al. [7] showed that it was indeed possible – at least on the Ge substrate on which the graphene was grown and whose specific properties enabled the formation of graphene nanobubble (GNB). Their work demonstrated programmable creation of GNB by applying negative tip voltage in AFM mode on graphene film grown on Ge (110) substrate by chemical vapor deposition (CVD). According to their findings, GNB are expected to be produced by voltage excited AFM tips from CVD graphene over clean Ge (110) substrate due to the low Ge–H bond energy. The weak Ge–H bond facilitates desorption of hydrogen atoms from the substrate under a local electric stimulus with negative tip bias. The hydrogen then forms H_2 molecules and fills the GNB as the surrounding graphene acts as an impenetrable enveloping layer. Is a Ge substrate necessary, or is a similar result can be achievable with transferred graphene using standard substrates? Here, we attempt this tackle this problem and we demonstrate the creation of nanobubbles in transferred graphene onto 285 nm SiO_2/Si substrate by applying electric field through the AFM tip and present an in-situ piezo-effect investigation of the created GNB.

2. Experimental part

2.1. Sample preparation

Preparation of graphene film was carried out using a standard method [29–31] in a closed chemical CVD chamber Nanofab (Oxford Instruments) on a 25 mm-thick copper foil (99.9%, MTI corporation). Before the deposition, the Cu Foil was cleaned in a mild ultrasonication bath consecutively for 10 min with de-ionised (DI) water, followed by isopropyl alcohol and finally in DI water again before letting it dry and flushing with nitrogen gun to remove all contaminants and particulates from the surface. Henceforth, the foil was first annealed at 1000 °C under 10^{-4} mbar and 5 sccm Ar flow for 30 min. Afterwards the Cu foil exposed to the mixture of hydrogen and methane in 1:7 ratio for 30 min to grow graphene. The process was finished by a slow cooling process to room temperature. Subsequently, the graphene films were transferred to the target substrate, 285 nm thick SiO_2 film on Si substrate, using a wet transfer method. The wet transfer method forms a crucial process to ensure transfer of CVD grown graphene into target substrates without contaminant residues of the adhesion layer and introducing defects in the graphene. Generally, poly methyl methylacrylate (PMMA) is a standard organic polymer used as a thin adhesion layer during wet transfer of graphene [32–34]. However, it is often observed that PMMA residues tend to stick to the graphene surface as contaminants even after its removal using organic solvents which affects the quality of the transferred graphene [35]. Hence, in order to circumvent this issue, we have chosen rosin based wet transfer method [36] instead of PMMA in the current context to achieve high quality of transferred graphene.

A thin layer of rosin (Alfa-Aesar, dissolved in ethyl lactate with a concentration of 50 wt%) was spin-coated on the CVD-grown graphene film at 500 r.p.m. for 10 s and 1200 r.p.m. for 60 s. Then, the rosin layer was air dried at room temperature for 24 h followed by etching the Cu foil in an aqueous solution of ammonium persulfate to obtain a rosin/graphene stack floating on the solution. After that, the rosin/graphene stack was collected on the target substrate and taken out from the solution. The rosin/graphene/target substrate was first treated at 40 °C for 1 h, and then the temperature was slowly increased to 120 °C during the next 20 min to evaporate the residual water. Finally, the rosin layer was dissolved by acetone (Analytical reagent, 99%) and isopropyl alcohol solutions (Analytical reagent, 99%) in sequence and then flushed using high-purity nitrogen for drying and residual of the unwanted surface residues before characterizations [36].

2.2. Piezoelectric force microscopy

Bruker Dimension ICON system was utilized to create approximately 100 GNBs by applying electric potential through the piezolectric force microscopy (PFM) tip to measure the morphologies and PFM response at ambient conditions. For the graphene bubbles fabrication, antimony doped Si AFM tips (SCM-PIT V2, Bruker) with spring constant 3 N/m were chosen. PFM images were acquired at resonant a.c. voltage (265 kHz) with the amplitude a.c voltage at 3 V. All the images were processed using open-source software package Gwyddion [37]. The correlation length T was calculated as the distance at which the one-dimensional autocorrelation function along the scan lines of the surface topography decays to 1/e. The bubble height h_{max} was computed as the difference between maximum and minimum height within the marked bubble area, its lateral radius as the radius of a circle with the same area. For the d_{33eff} evaluation we used the same ramp voltage as for the bubble creation and to extract the amplitude displacement correlations from the PFM hysteresis loop.

2.3. Raman spectroscopy

Raman spectroscopy was performed in a standard micro-Raman set up (Alpha 300R) from Witec, GmbH. The spectra were collected in a backscattered geometry with beam diameter (1 μm) and 100× Zeiss objective (NA = 0.9) using linearly polarized 532 nm laser excitation source with a 600 gr/mm optical grating.

3. Results and discussion

At first, we tracked the evolution of graphene topography from a CVD graphene film on a 285 nm SiO_2/Si in a time series scan using PFM mode under resonant frequency condition (265 kHz) with a static −3 V tip bias (no observable changes were found below −3 V). Repeated scanning slowly modified the SLG topography (Fig. 1ab). We quantified the change in surface morphology using the correlation length (T). After an initial scan performed without a driving voltage, T increased slightly for the first PFM scan, which could be attributed to changes in tip-sample interactions. Then, it systematically decreased after each scan, approximately following the dependence $T(n) = (an + b)/(1 + cn)$, where n is the number of times the surface was scanned (Fig. 1c) and a, b and c are constants. Interestingly, only the characteristic lateral dimensions of the wrinkles, i.e. the correlation length, were changing. Parameters characterizing their vertical scale (such as average or root mean square roughness) remained constant. The modification of graphene topography under the tip voltage is consistent with

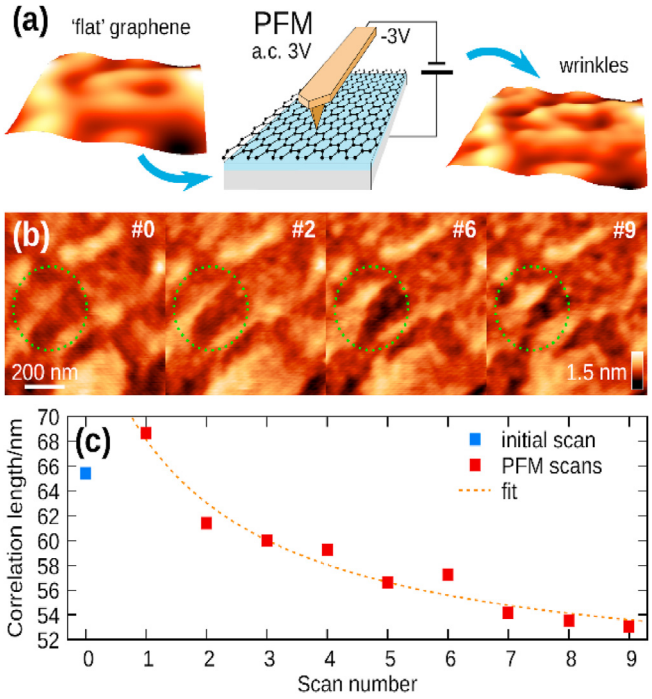

Fig. 1. Formation of graphene nanobubbles under applied tip voltage (a) Schematic representation showcasing the change in graphene morphology when potential is applied through the PFM tip (b) Snapshots depicting the evolution in the topography of graphene surface under constant voltage tip bias −3V and resonant peak frequency condition in a time series scan. The pseudocolor mapping range is the same for all images. The dashed green circle is a guide to the eye showing the region where prominent changes in the morphology is observed (c) Change of correlation length as a function of number of image scan fitted by a linear rational function.

previous observations [28] which suggests more formation of folds/wrinkles in graphene with time and that strain engineering is possible using the AFM tip. It also underlines that in electrical modes we do not just measure the graphene, we also often modify it, in particular when one region is scanned repeatedly.

Next, we focused on a strategy to create GNB using the AFM tip. We initially attempted to follow a previously reported protocol by Jia et al. [7]. The protocol demonstrated programmable creation of GNBs by applying negative tip voltage in AFM mode on CVD grown graphene film deposited on Ge (110) substrate. According to their findings, GNBs are expected to be produced by voltage excited AFM tips from CVD graphene only over clean Ge (110) substrate due to the low Ge−H bond energy. However, in our case, under a fixed bias to the AFM tip and scanning the SLG surface. it did not produce any GNB. In our strategy, the creation of GNB was only possible when the resonant frequency (265 kHz) a.c. voltage at 3V was applied to the AFM tip in combination with a negative or positive bias or a ramp d.c. voltage (from -2V to 2V, -4V−4V, …, −12V−12V). A point was selected in the center of a flat graphene surface area and the tip voltage was applied for ~4 min (wait time) before rescanning the same area again to image the newly created GNB. Under the static bias conditions (no ramp), the production of GNB was not reliable, especially for applied positive bias. We found that the best condition, in which the GNBs were most consistently produced and most homogeneous in shape, was the ramp d.c. voltage mode combined with the a. c. resonant frequency voltage (3 V). We believe that a ramp voltage facilitates in poling or 'pre-stressing' the graphene surface in a more effective way by varying the voltage from a minimum to a maximum. This helps to orient the direction of the dipoles accordingly thus creating a more uniform shaped bubble.

Our observation suggests that GNB can be created using in situ by AFM tip under the electric field on transferred graphene as we successfully obtained them on the standard SiO_2/Si substrates. We believe that the transfer of CVD graphene on a substrate generate more wrinkles and thereby impacting the final shape of the bubble under the applied field. The wrinkles are intrinsic part of surface grown CVD graphene. This is often caused by the difference in thermal expansion coefficients between graphene and the underlying substrate in the cooling process after high temperature growth. Other conditions can include the surface roughness of the substrate on which graphene is grown [38,39]. Furthermore, when transferring CVD graphene on SiO_2/Si substrates, some air containing several types of molecules gets trapped inside which can further generate larger wrinkles or bubbles. These molecules could be positively or negatively charged. There have several reports where the mechanical properties and stability of bubbles have been studied in great details by filling the interior with liquids/gases and under pressurized conditions [40–46] Moreover, depending on the polarity of the voltage applied through the AFM tip to induce the electric field on the surface of SLG, one may very well expect the selective desorption of gases to form the GNB which is reported previously [7]. We also found that the wait time during which the tip voltage was maintained on the SLG surface only influenced whether GNB were reliably produced (for ~ 4 min) or not (for ~30 s). However, it did not influence the physical attributes of the formed GNBs as much as the tip voltage and the tip distance did.

3.1. Bubble geometry

Fig. 2a shows the evolution of the GNB formed at different ramp voltages applied to the tip. Their physical attributes such as area A, maximum height h_{max} and volume V are plotted in Fig. 2b as functions of the ramp voltage (±2−±12V) for a constant tip distance D of ~20 nm. All the parameters characterizing the size of the nanobubbles generally increased with increasing the ramp voltage. However around ~ ±8V a plateau or even a slight decrease seems to have occurred. The same parameters were determined for the GNBs created using the fixed ramp voltage ±12V but varying the tip distance D from 40−100 nm (Fig. 2c and d). All three size parameters decreased with the distance. The height and volume decreased more or less linearly, and their linear fits led to the conclusion that the GNB would cease to be produced beyond D_{max} ~140 nm. The fits gave $D_{max} = 130 \pm 22$ nm from the bubble height and $D_{max} = 141 \pm 5$ nm from the volume. In contrast, the area A decreased with D only up to D ~50 nm but remained approximately the same for larger distances.

The shape of the bubbles is related to the adhesion energies due to van der Waals (vdW) interactions between graphene and the underlying substrate. For zero stress ($\varepsilon = 0$), it should follow a universal scaling law $h_{max}/R = \left(\frac{\pi\gamma}{5cY}\right)^{1/4}$ where R is the bubble radius, γ is the adhesion energy between the SLG and the substrate (SiO_2/Si), Y is the Young's modulus and $c = 0.7$ [7,44,45]. The aspect ratio h_{max}/R is plotted in Fig. 3a for the GNB over a wider range of ramp voltages as a function of the nanobubble radius. Previously, h_{max}/R was found to be 0.08–0.11 for $R > 50$ nm, or 0.18 for small GNB filled with helium gas in the graphene interlayer. In our case, we found a wide range of aspect ratios due to a more varied GNB shape. Nevertheless, the average value ~0.07 matches closely the previously obtained results and indicates the adhesion energy between the underneath substrate and the graphene layer is small [7]. In addition, we analyzed the shape of the base contour radius (R), as a function of the height under different applied ramp voltages and at the constant 20 nm tip distance. It is argued that for the smaller GNB, with radii $R < 50$ nm, the bottom part of the base could be fitted by a parabolic

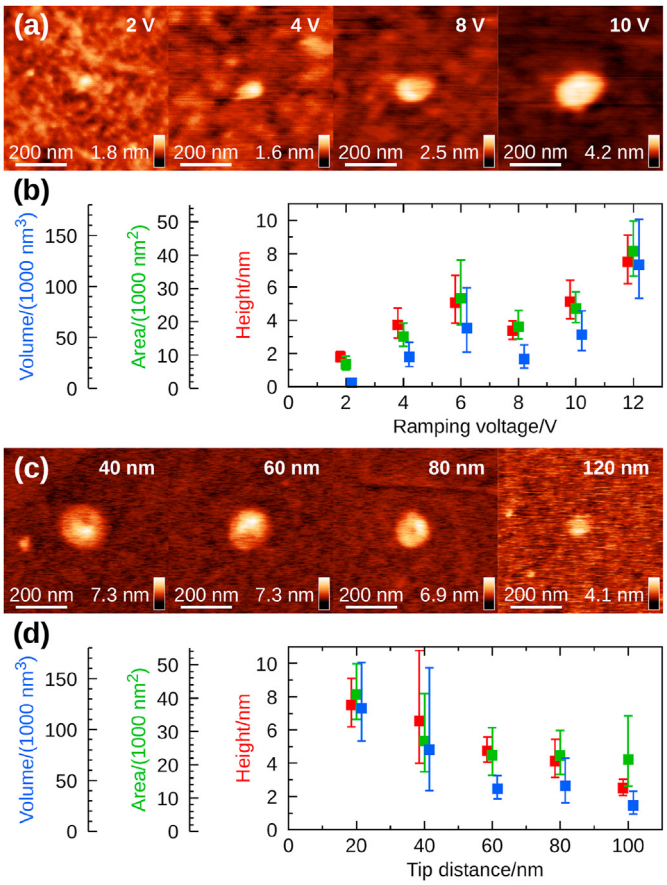

Fig. 2. Evolution of GNB as a function of applied tip voltage and tip distance (a) Topography of newly created GNB formed under different ramp voltage conditions (b) Dependence of height, area, and volume of the newly created GNB as a function of increasing ramp voltage from ±2 to ±12V (c) Topography of newly created GNB formed under different tip distance conditions (d) Dependence of height, area, and volume of the newly created GNBs as a function of increasing tip distance from 20 to 100 nm under fixed ramp voltage ±12V

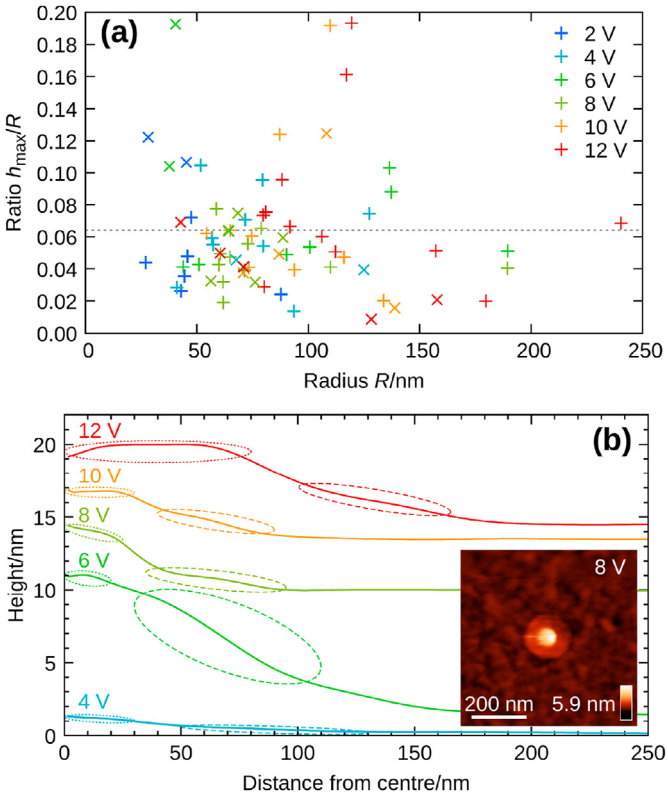

Fig. 3. Aspect Ratio and radial base profile of GNB (a) Aspect ratios of GNB as a function of the base radius under different applied tip voltage (ramp mode). The gray line shows the mean value ~0.07. (b) Radial profiles extracted from nanobubbles formed under different ramp voltages. The dotted circles act as a guide to the eye to depict that the shape of the radial profile mostly following a mixed Gaussian and parabolic distribution. The inset figure shows one such example of GNB having a mixed radial profile distribution formed under applied ramp voltage ~±8V

function $z(r) = h_{max}(1 - r^2/R^2)$, where h_{max} is the maximum height from the base and R is the radius of the bubble in accordance with the membrane model [47]. However, in our case, the top part (apex) in most of the nanobubbles transformed to a Gaussian profile described by the equation $z(r) = h_{max}\exp(-r^2/2\sigma^2)$, where σ is the width of the Gaussian profile. This change of the radial profile from the base to the top apex for larger GNB ($R \geq 50$nm) was observed previously [7] and is mainly attributed to the weakening of the vdW interactions, which strongly varies with the distance between the substrate and graphene as the radius of GNB changes. Selected radial profiles of the GNB are plotted from ±2 to ±12V (ramp voltage) to reveal this complex relationship as shown in Fig. 3b.

3.2. Piezoresponse

The measured piezoresponse of a 2D material can be classified as piezoelectric or flexoelectric in nature. Piezoelectricity is described by a third-order tensor resulting from uniform strain mainly consists of 'in-plane' polarization and sometimes accompanied by 'out of plane' polarization [17,48]. On the other hand, flexoelectricity is defined strictly as strain gradient–induced polarization or electric gradient–induced strain in crystalline solids, described by the fourth-order tensor explicitly generating out of plane (vertical) polarization only in the z-direction [17,19]. Furthermore, flexoelectricity has no crystallographic constraint [48], but a large strain gradient is needed to observe it. This is more feasible at nanoscale material where a large gradient can be achieved by a small strain [18]. The polarization tensor can be written as $P_i = e_{ijk}\varepsilon_{jk} + f_{ijkl}\partial\varepsilon_{jk}/\partial x_l$, where ε_{jk} is elastic strain ($e_{ijk}\varepsilon_{jk} = 0$ for non-piezo materials),e_{ijk} is the piezoelectric coefficient) and f_{ijkl} is the flexoelectric coefficient [48–50]. Hence, even in the absence of native piezoelectricity, the polarization exists due to non-uniform strain, breaking the inversion symmetry and forming electromechanical couplings. In recent reports, Kang et al. [19] mentioned the role of surface corrugations in the generation of strain gradients in $MoTe_2$ for out-of-plane flexoelectricity, which is also relevant for the GNB. Hence, the generation of piezoresponse and flexoelectricity in modified graphene structures is plausible.

In Fig. 4abc, we show the PFM images (topography, phase, and amplitude) measured as out of plane (vertical) piezoresponse of a GNB created using ±10 V ramp and 20 nm tip distance. During our measurements, no conclusive evidence of in-plane piezoresponse was observed. We attribute the out of plane piezoresponse in the GNB purely to flexoelectricity. It is evident from the images that the shape of the nanobubble has a uniform slightly elongated contour with good out-of-plane phase and inverted amplitude contrast due to electromechanical coupling. As a measure of quantifiable out of plane piezoresponse or flexoelectricity under the electric field, the PFM signal calculates the piezoelectric coefficient d_{33} from PFM signals. However, experimental uncertainties because of other contributing factors such as electromechanical effects, electrostatic effects, instrumental noise and topographical artifacts are always

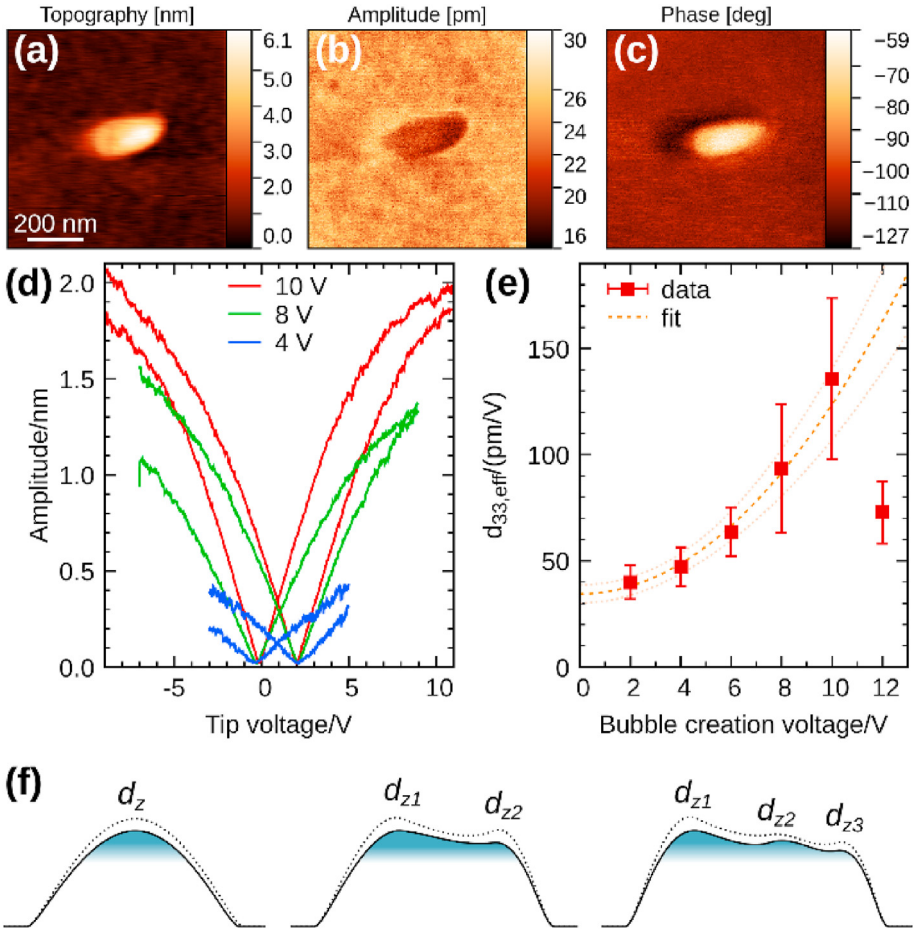

Fig. 4. PFM response of the GNB (a) Topography, (b) Amplitude and (c) Phase image; (d) Amplitude displacement dependence as a function different ramp voltage. Driving a.c. voltage is 3V at frequency ~265 kHz (e) Relationship between d_{33eff} calculated from (d) as a function of bubble creation voltage (ramp voltage) with fitted quadratic dependence for voltage <±12V (95% confidence intervals) (f) Schematic representation of local distribution of the strain gradients (d_z) depending on the shape and the radial profile of the bubbles under applied electric field.

present. Hence, in actual PFM experiments, it is popularly defined as the effective piezoelectricity coefficient (d_{33eff}) [17]. There are several methodologies reported in literature to evaluate the piezoelectric coefficient in 2D materials.[8,9,17,20,48]. We estimated the maximum effective piezoelectric coefficient d_{33eff} to be 0.13 nm/V from the linear portion of the PFM hysteresis loop (Fig. 4d) in the nanobubbles [51]. Furthermore, we find that d_{33eff} increases as a function of bubble creation voltage (ramp voltage) as shown in Fig. 4de. For V < ±12 V, it can be fitted with a simple quadratic function of the type $d_{33eff} = d_0 + cV^2$, where d_0 and c are constants (Fig. 4e). The value for ±12 V (ramp mode) lies clearly outside this trend as the coefficient seems to decrease again. A possible explanation could be is that the highest voltage induces substantial strain and thereby the GNBs undergo a structural relaxation at the apex forming kinks/dents (supplementary information), which in turn reduces the d_{33eff} observed after GNB creation. In Fig. 4f, we provide a schematic representation to illustrate the out-of-plane piezo-effect in the nanobubbles. We surmise that the d_{33eff} obtained for the different bubbles corresponds to the average of all the local strain gradient displacements depending on the radius or the shape of the bubbles under applied electric field.

4. Conclusions

We have created graphene nanobubbles in the single layer graphene transferred on the traditional SiO_2/Si substrate by applying ramping voltage through the AFM tip. We investigated the dimensional parameters (height, area and volume) of the nanobubbles as a function of the ramp voltage and tip distance. All three-dimensional parameters seem to increase with increasing ramp voltage but decreased with increasing tip distance except for the area which remained constant beyond distance of 50 nm. Furthermore, we confirm that the creation of GNB by AFM tip can be independent of the underlying substrate and controllability of the dimensional parameters is possible with transferred graphene. We used PFM technique to measure the out of plane piezoresponse or flexoelectricity in the nanobubbles resulting from the non-uniform strain gradient distributed within the nanobubbles with complementary phase-amplitude contrast. We estimate the maximum d_{33eff} from the PFM signal ~0.13 nm/V and observe quadratic dependence with increasing bubble creation voltage. We believe our work provides an impetus for creation of nanobubbles with AFM tip under electric field to probe the flexoelectric properties with other 2D materials such as MoS_2, WS_2 etc. transferred on different substrates for potential piezoelectric applications.

CRediT authorship contribution statement

Rajarshi Roy: Conceptualization, Methodology, Investigation, Validation, Writing – original draft, Supervision, Project

administration. **David Nečas:** Software, Formal analysis, Writing – review & editing, Visualization. **Lenka Zajíčková:** Writing – review & editing.

Declaration of competing interest

The authors declare that they have no known financial interests/personal relationships that could have appeared to influence the work reported in this paper.

Acknowledgements

RR would like to acknowledge funding by European Regional Development Fund-Project "MSCAfellow2@MUNI" (No. CZ.02.2.69/0.0/0.0/18_070/0009846). We acknowledge CzechNanoLab Research Infrastructure supported by MEYS CR (LM2018110) to carry out this research. The authors would like to acknowledge Petr Klapetek from Czech Metrology Institute, Brno, Czech Republic, Markus Kratzner from Montanuniversität, Leoben, Austria, Subhajit Saha from Institute of Biomedical Engineering, National Tsing Hua University, Hsinchu, Taiwan, Marek Eliáš and Radim Zahradníček from CEITEC Nano, BUT, Brno, Czech Republic for helpful discussions during this work.

References

[1] A.K. Geim, Graphene: status and prospects, Science 324 (2009) 1530–1534.
[2] X. Li, L. Colombo, R.S. Rouff, Graphene films: synthesis of graphene films on copper foils by chemical vapor deposition, Adv. Mater. 28 (2016) 6247–6252.
[3] T. Georgiou, L. Britnell, P. Blake, R.V. Gorbachev, A. Gholinia, A.K. Geim, C. Casiraghi, K.S. Novoselov, Graphene bubbles with controllable curvature, Appl. Phys. Lett. 99 (2011), 093103.
[4] J. Lu, A.H. Castro Neto, K.P. Loh, Transforming moiré blisters into geometric graphene nano-bubbles, Nat. Commun. 3 (2011) 823.
[5] Y. Huang, X. Wang, X. Zhang, X. Chen, B. Li, B. Wang, et al., Raman spectral band oscillations in large graphene bubbles, Phys. Rev. Lett. 120 (2018) 186104.
[6] N. Levy, S.A. Burke, K.L. Meaker, M. Panlasigui, A. Zettl, F. Guinea, et al., Strain-induced pseudo–magnetic fields greater than 300 tesla in graphene nanobubbles, Science 329 (2010) 544.
[7] P. Jia, W. Chen, J. Qiao, M. Zhang, X. Zheng, Programmable graphene nanobubbles with three-fold symmetric pseudo-magnetic fields, Nat. Commun. 10 (2019) 3127.
[8] G. da Cunha Rodrigues, P. Zelenovskiy, K. Romanyuk, S. Luchkin, Y. Kopelevich, A. Kholkin, Strong piezoelectricity in single-layer graphene deposited on SiO_2 grating substrates, Nat. Commun. 6 (2015) 7572.
[9] X. Wang, H. Tian, W. Xie, Y. Shu, W.T. Mi, M.A. Mohammad, Q.Y. Xie, Y. Yang, J.B. Xu, T.L. Ren, Observation of a giant two-dimensional band-piezoelectric effect on biaxial-strained graphene, NPG Asia Mater. 7 (2015) 154.
[10] C. Si, Z. Sun, F. Liu, Strain engineering of graphene: a review, Nanoscale 8 (2016) 3207–3217.
[11] S.I. Kundalwal, S.A. Meguid, G.J. Weng, Strain gradient polarization in graphene, Carbon 117 (2017) 462.
[12] B. Javvaji, B. He, X. Zhuang, The generation of piezoelectricity and flexoelectricity in graphene by breaking the materials symmetries, Nanotechnology 29 (2018) 225702.
[13] S.V. Kalinin, V. Meunier, Electronic flexoelectricity in low-dimensional systems, Phys. Rev. B 77 (2008), 033403.
[14] W. Shi, Y. Guo, Z. Zhang, W. Guo, Flexoelectricity in monolayer transition metal dichalcogenides, J. Phys. Chem. Lett. 9 (2018) 6841.
[15] R. Hinchet, U. Khan, C. Falconi, S.-W. Kim, Piezoelectric properties in two-dimensional materials: simulations and experiments, Mater. Today 21 (2018) 611.
[16] M.N. Blonsky, H.L. Zhuang, A.K. Singh, R.G. Hennig, Ab initio prediction of piezoelectricity in two-dimensional materials, ACS Nano 9 (10) (2015) 9885–9989.
[17] C.J. Brennan, R. Ghosh, K. Koul, S.K. Banerjee, N. Lu, E.T. Yu, Out-of-Plane electromechanical response of monolayer molybdenum disulfide measured by piezoresponse force microscopy, Nano Lett. 17 (9) (2017) 5464–5471.
[18] C.J. Brennan, K. Koul, N. Lu, E.T. Yu, Out-of-plane electromechanical coupling in transition metal dichalcogenides, Appl. Phys. Lett. 116 (2020), 053101.
[19] S. Kang, S. Jeon, S. Kim, D. Seol, H. Yang, J. Lee, Y. Kim, Tunable out-of-plane piezoelectricity in thin-layered $MoTe_2$ by surface corrugation-mediated flexoelectricity, ACS Appl. Mater. Interfaces 10 (2018) 27424–27431.
[20] X. Wang, A. Cui, F. Chen, L. Xu, Z. Hu, K. Jiang, L. Shang, J. Chu, Probing effective out-of-plane piezoelectricity in van der Waals layered materials induced by flexoelectricity, Small 15 (2019) 1903106.
[21] P. Ares, T. Cea, M. Holwill, Y.B. Wang, R. Roldán, et al., Piezoelectricity in monolayer hexagonal boron nitride, Adv. Mater. 32 (2020), 1905504.
[22] H. Rostami, F. Guinea, M. Polini, R. Roldán, Piezoelectricity and valley chern number in inhomogeneous hexagonal 2D crystals, NPJ 2D Mater. Appl. 2 (2018) 15.
[23] B. Wang, S. Yang, P. Sharma, Flexoelectricity as a universal mechanism for energy harvesting from crumpling of thin sheets, Phys. Rev. B 100 (2019), 035438.
[24] X. Zhuang, B. He, B. Javvaji, H.S. Park, Intrinsic bending flexoelectric constants in two-dimensional materials, Phys. Rev. B 99 (2019), 054105.
[25] F. Ahmadpoora, P. Sharma, Flexoelectricity in two-dimensional crystalline and biological membranes, Nanoscale 7 (2015) 16555.
[26] J.K. Hana, S. Kim, S. Jang, Y.R. Lima, S.-W. Kim, et al., Tunable piezoelectric nanogenerators using flexoelectricity of well-ordered hollow 2D MoS2 shells arrays for energy harvesting, Nanomater. Energy 61 (2019) 471.
[27] S.-J. Tsai, C-Lin Wu, N.-T. Tsai, S.-S. Wong, L.-W. Tu, Epitaxy of obliquely aligned GaN nanorods on vertically oriented graphene nanosheets for transparent flexible piezoelectric nanogenerators, Carbon 130 (2018) 390.
[28] C. Musumeci, Advanced scanning probe microscopy of graphene and other 2D materials, Crystals 7 (2017) 216.
[29] S. Bae, H. Kim, Y. Lee, X. Xu, J.S. Park, et al., Roll-to-roll production of 30-inch graphene films for transparent electrodes, Nat. Nanotechnol. 5 (2010) 574–578.
[30] X. Li, W. Cai, J. An, S. Kim, J. Nah, Large-area synthesis of high-quality and uniform graphene films on copper foils, Science 324 (2009) 1312–1314.
[31] J. Jang, M. Son, S. Chung, et al., Low-temperature-grown continuous graphene films from benzene by chemical vapor deposition at ambient pressure, Sci. Rep. 5 (2015) 17955.
[32] S. Kim, S. Shin, T. Kim, H. Du, M. Song, et al., Robust graphene wet transfer process through low molecular weight polymethylmethacrylate, Carbon 98 (2016) 352.
[33] X. Yang, M. Yan, Removing contaminants from transferred CVD graphene, Nano Res 13 (2020) 599.
[34] A. Suhail, K. Islam, B. Li, D. Jenkins, G. Pan, Reduction of polymer residue on wet–transferred CVD graphene surface by deep UV exposure, Appl. Phys. Lett. 110 (2017) 183103.
[35] G. Deokar, J. Avila, I. Razado-Colambo, J.-L. Codron, C. Boyaval, Towards high quality CVD graphene growth and transfer, Carbon 89 (2015) 82.
[36] Z. Zhang, J. Du, D. Zhang, H. Sun, L. Yin, L. Ma, J. Chen, D. Ma, H.M. Cheng, W. Ren, Rosin-enabled ultraclean and damage-free transfer of graphene for large-area flexible organic light-emitting diodes, Nat. Commun. 8 (2017) 14560.
[37] D. Nečas, P. Klapetek, Gwyddion: an open-source software for SPM data analysis, Cent. Eur. J. Phys. 10 (2012) 181.
[38] N. Liu, Z. Pan, L. Fu, C. Zhang, B. Dai, Z. Liu, The origin of wrinkles on transferred graphene, Nano Res 4 (2011) 996.
[39] S. Deng, V. Berry, Wrinkled, rippled and crumpled graphene: an overview of formation mechanism, electronic properties, and applications, Mater. Today 19 (2016) 197.
[40] D.A. Sanchez, Z. Dai, P. Wang, A. Cantu-Chavez, C.J. Brennan, R. Huang, N. Lu, Mechanics of spontaneously formed nanoblisters trapped by transferred 2D crystals, Proc. Natl. Acad. Sci. Unit. States Am. 115 (2018) 7884.
[41] G. Zamborlini, M. Imam, L.L. Patera, T.O. Mentes, N. Stojic, et al., Nanobubbles at GPa pressure under graphene, Nano Lett. 15 (2015) 6162.
[42] S.K. Jain, V. Juričic, G.T. Barkema, Probing the shape of a graphene nanobubble, Phys. Chem. Chem. Phys. 19 (2017) 7465.
[43] K.M. Zahra, C. Byrne, A. Alieva, C. Casiraghi, A.S. Walton, Intercalation, decomposition, entrapment – a new route to graphene nanobubbles, Phys. Chem. Chem. Phys. 22 (2020) 7606.
[44] D. Shin, J.B. Park, Y.-J. Kim, S.J. Kim, J.H. Kang, et al., Growth dynamics and gas transport mechanism of nanobubbles in graphene liquid cells, Nat. Commun. 6 (2015) 6068.
[45] E. Khestanova, F. Guinea, L. Fumagalli, A.K. Geim, I.V. Grigorieva, Universal shape and pressure inside bubbles appearing in van der Waals heterostructures, Nat. Commun. 7 (2016) 12587.
[46] H. Ghorbanfekr-Kalashami, K. Vasu, R. Nair, F.M. Peeters, M. Neek-Amal, Dependence of the shape of graphene nanobubbles on trapped substance, Nat. Commun. 8 (2017) 15844.
[47] K. Yue, W. Gao, R. Huang, K.M. Liechti, Analytical methods for the mechanics of graphene bubbles, J. Appl. Phys. 112 (2012), 083512.
[48] M. Zelisko, Y. Hanlumyuang, S. Yang, Y. Liu, C. Lei, J. Li, P.M. Ajayan, P. Sharma, Anomalous piezoelectricity in two-dimensional graphene nitride nanosheets, Nat. Commun. 5 (2014) 54284.
[49] L. Shu, X. Wei, T. Pang, X. Yao, C. Wang, Symmetry of flexoelectric coefficients in crystalline medium, J. Appl. Phys. 110 (2011) 104106.
[50] S. Chandrantre, P. Sharma, Coaxing graphene to be piezoelectric, Appl. Phys. Lett. 100 (2012), 023114.
[51] S. Salemizadeh Parizi, A. Mellinger, G. Caruntu, Ferroelectric barium titanate nanocubes as capacitive building blocks for energy storage applications, ACS Appl. Mater. Interfaces 6 (20) (2014) 17506–17517.